16th World Congress in Computational Mechanics (WCCM)
21-26 July 2024, Vancouver, Canada
A. Korobenko, M. Laforest, S. Prudhomme, R. Vaziri (Eds)

MODELING THE ENHANCED GEOTHERMAL SYSTEMS USING THE EXTENDED–FEM AND AN EQUIVALENT CONTINUUM MODEL

AMIR R. KHOEI [1], MOHAMMAD S. MORTAZAVI [2], OMID R. BEYDOKHTI [3] AND POORYA PIRMORADI [4]

Center of Excellence in Structures and Earthquake Engineering, Department of Civil Engineering, Sharif University of Technology, P.O. Box. 11365-9313, Tehran, Iran
[1] arkhoei@sharif.edu and https://sharif.edu/~arkhoei/

Key words: Thermo-Hydro-Mechanical model; Enhanced geothermal systems; Local thermal non-equilibrium; XFEM; Equivalent continuum method.

Abstract. In this paper, a computational technique is presented for Thermo-Hydro-Mechanical (THM) simulation of Enhanced Geothermal Systems (EGS) based on the eXtended Finite Element Method (XFEM) and Equivalent Continuum Method (ECM) in the framework of Local Thermal Non-Equilibrium (LTNE). Heat extraction from Enhanced Geothermal Systems involves several multi-physics coupling processes, including the seepage through the fractured porous media, the thermal exchange between the working fluid and the matrix, and the deformation of fractured porous media that play essential roles in exploiting the geothermal energy contained in hot dry rocks. The ECM provides the equivalent tensors for the fluid permeability and solid compliance, which is an essential feature for the coupled Thermo-Hydro-Mechanical simulation of fracture networks. In the model, the XFEM is employed for large-scale fractures to capture the mass and heat transfer between the fracture and matrix more accurately, while the ECM is applied on the network of small-scale fractures. Hence, the proposed model benefits from the advantages of both methods, and it allows for managing between accuracy and cost. The set of THM equations is solved with both Local Thermal Equilibrium (LTE) and Local Thermal Non-Equilibrium (LTNE) assumptions to find out the impact of each method on the production temperature. The capability of the proposed computational model is demonstrated for the diagonal arrangement of the injection and production wells with different fracture orientations in-between. The simultaneous effects of fracture connectivity and inclination are investigated between the two injection and production wells. It is observed that the temperature difference between the two cases is higher in the middle of the domain by comparing the results of LTE and LTNE assumptions. Moreover, it is concluded that the LTE model overestimates the fluid temperature in comparison to the LTNE model in cold water injection problems. The results show the proposed computational model is a promising tool for estimation of the heat mining performance of EGS.

1 INTRODUCTION

Geothermal energy is mostly stored in hot dry rocks (HDR), which are tight formations deeply buried 1-5 kilometers underground with sufficient heat content [1]. Due to low permeability and water content, the HDR mass is difficult to be exploited with the conventional methods [2]. Hence, the hydraulic stimulation technologies are used in EGS to increase the connectivity between wells through low-permeability reservoirs in the HDR mass [3]. The energy is then extracted by circulating cold water from the injection wells to the production wells and extracting the heated water to generate power. The usage of EGS can help to extend the geothermal resources and to improve the productivity [4]. The geothermal energy development and operation involve several multi-physics processes, such as rock deformation and stress alteration, fluid flow, and temperature change in the fractured rock mass, which are called the Thermo-Hydro-Mechanical (THM) coupled processes [5]. Therefore, the THM coupled simulation can be useful in estimation of the efficiency of EGS projects.

The computational models of geothermal problems are usually proposed based on the Thermo-Hydraulic (TH) or Thermo-Hydro-Mechanical (THM) model. Clearly, the mechanical effects are often crucial and cannot be disregarded in EGS assessment. It can be inferred from the essential role of fracture aperture in the energy extraction rate from EGS reservoirs. In fact, neglecting the mechanical effects can overestimate the output thermal power [6]. The effects of the fracture network characteristics on the results of EGS simulation were investigated in [7]. It is shown that increasing the matrix permeability can increase the fluid leak-off from the fractures. It reduces the fluid velocity, and increases the period of hot water production. Moreover, it was revealed that assuming a variable heat transfer coefficient between the fluid and solid phases increases the production temperature compared with considering it constant [8]. The matrix block in EGS usually consists of fractures with different length scales. The incorporation of fractures within the numerical model can increase the computational cost noticeably. The Equivalent Continuum Model (ECM) is appropriate for modeling networks of short cracks, and has a relatively low computational cost. In this method, fractures are modeled implicitly by exporting their hydro-mechanical properties to an equivalent macro-scale continuum. The stiffness and permeability matrices of the continuum are modified based on the fractures' characteristics. Alternatively, the long fractures can be modeled explicitly using the eXtended Finite Element Method (XFEM). The XFEM was established by locally enriching the standard FEM functions under the Partition of Unity concept. The technique was employed through a THM model to investigate the propagation of fractures in unsaturated porous media under non-isothermal conditions [9]. Moreover, a combined XFEM–ECM model was applied on TH problems of unsaturated porous media to study the isothermal and non-isothermal water flooding into fractured oil reservoirs [10]. In this study, a hybrid XFEM–ECM model is employed in fully coupled THM simulations of EGS. The coupling of THM equations is reflected via the coupling terms in the governing equations, and the coupling between the fracture and matrix is considered by a unified discretization approach in the XFEM. The proposed model benefits from the advantages of both methods, and it allows for managing between accuracy and cost.

In the THM analysis of EGS, an assumption may be considered based on the instantaneous thermal equilibrium between the fluid and solid phases in the porous medium. This assumption

simplifies modeling since a single temperature field is sufficient to be solved. However, this assumption cannot be applied when the time of adjacency of the fluid particles to the solid particles is relatively short; and the equilibrium temperature cannot be reached by the phases. Hence, the Local Thermal Non-Equilibrium (LTNE) has been proposed instead of the Local Thermal Equilibrium (LTE) in several studies of geothermal energy extraction [11]. It was shown that the problem specifications, such as the fluid velocity and the coefficient of heat transfer between the phases, can intensify the effects of LTNE assumption and change the thermal breakthrough time. In the current study, a computational algorithm is presented by extending the formulation to LTNE, adding the mechanical part of ECM to the formulation, and implementing the contact algorithm of XFEM, to make it eligible for EGS simulations. To this end, the fractures are classified based on their length and distribution, where short fractures are modeled implicitly by the ECM, and larger fractures are modeled explicitly with the XFEM. The results of numerical simulation provide interesting findings about the effects of distribution and orientation of fractures in EGS. Moreover, the influences of the LTE and LTNE approaches, the connectivity of fractures, and the alteration of fluid properties are investigated. It is observed that the network connectivity and fracture alignment are both influential on the early thermal breakthrough; however, each can take dominance under different conditions.

2 GOVERNING EQUATIONS OF THE MATRIX DOMAIN

2.1 Linear momentum balance equation

The linear momentum balance equation of saturated porous media can be written as

$$\nabla \cdot \boldsymbol{\sigma} - \rho \ddot{\mathbf{u}} + \rho \mathbf{b} = 0 \tag{1}$$

where $\ddot{\mathbf{u}}$ is the acceleration of solid phase, $\mathbf{b}$ is the body force, ρ is the average density of mixture defined by $\rho = n\rho_w + (1-n)\rho_s$. Since the porous medium and solid grains are both assumed compressible, the effective stress can be defined by $\boldsymbol{\sigma}' = \boldsymbol{\sigma} + \alpha \mathbf{m} p$, in which $\boldsymbol{\sigma}$ is the total stress, $\boldsymbol{\sigma}'$ the effective stress, α the Biot coefficient, and $\mathbf{m}$ is defined as $\mathbf{m} = [1\ 1\ 0]^{\mathrm{T}}$. In case of linear elastic behavior, the stress-strain relation is defined as $\boldsymbol{\sigma}' = \mathbf{D}(\boldsymbol{\varepsilon} - \boldsymbol{\varepsilon}_T)$, where $\mathbf{D}$ denotes the elastic constitutive matrix, $\boldsymbol{\varepsilon}$ is the strain vector, and $\boldsymbol{\varepsilon}_T$ is the thermal strain vector defined by $\boldsymbol{\varepsilon}_T = \frac{1}{3}\hat{\nu}\beta_S \theta \mathbf{m}$, with $\hat{\nu} = 1$ for the plane stress and $\hat{\nu} = (1+\nu)$ for the plane strain problems. The temperature difference $\theta = T_S - T_0$ is defined as the reference temperature.

2.2 Continuity of the fluid phase

The mass conservation equation of a single-phase flow in deformable porous media can be obtained by combining the continuity equations for each phase (solid and fluid) in the representative elementary volume. Assuming the fluid density as a function of pressure and temperature, the empirical relation of the fluid density can be written as [12]

$$\rho_w = \rho_0 \exp\left[-\beta_w T_w + \frac{1}{K_w(p - p_0)}\right] \tag{2}$$

where K_w is the bulk moduli of the fluid phase, $T_w(^{\circ}\mathrm{C})$ is the temperature of the fluid phase,

and β_w is the volumetric thermal expansion coefficient. Applying the above equation, the governing equation of the fluid continuity can be written as

$$\alpha \nabla \cdot \mathbf{v}_S + n \nabla \cdot \mathbf{u}_m + S_m \dot{p} - \beta_m \dot{T} = 0 \tag{3}$$

where α is the Biot coefficient, β_m is the bulk thermal expansion coefficient defined as $\beta_m = (\alpha - n)\beta_S + n\beta_W$, and the storage coefficient is defined as $S_m = (\alpha - n)/K_S + n/K_W$. In above, $\mathbf{v}_S$ is the solid velocity, $\mathbf{u}_m$ is the Darcy velocity of the fluid, n is the porosity, β_S and β_w are the volumetric thermal expansion coefficients and, K_S and K_W are the bulk moduli of the solid and fluid phases, respectively. According to Darcy's law, the fluid flux can be defined as

$$\mathbf{u}_m = \mathbf{k}_m \left(-\nabla p + \rho_w \mathbf{b} \right) \tag{4}$$

in which $\mathbf{k}_m$ is the permeability matrix defined as $\mathbf{k}_m = \mathbf{k}/\mu_w$, with $\mathbf{k}$ denoting the intrinsic permeability and μ_w the dynamic viscosity of the fluid. The empirical relation for evolutions of the dynamic viscosity with temperature is defined by $\mu_w = 1/\left(29.83(T_w + 14.55)\right)$ [13].

2.3 Energy conservation equation

The energy conservation equation of each phase can be applied in the same way as the mass conservation equation to derive the macro-scale relations of energy conservation in the LTE formulation; however, it cannot be the case in LTNE. In fact, the energy conservation equations of the solid and fluid phases are not averaged in the LTNE model, and they are solved separately by distinct main variables of the temperature. In the *Local Thermal Equilibrium* (LTE) formulation, it is assumed that the solid phase temperature gets instantaneously to the equilibrium condition with the fluid phase. On the other hand, the equilibrium takes place much faster than the heat transport processes. The heat transport equation for this model can be obtained by applying the averaging theory to the energy conservation of each phase, which renders the following equation

$$(\rho C)_{\text{avg}} \frac{\partial T}{\partial t} + \left(\rho_w C_w \mathbf{u}_m \right) \nabla T - \lambda_{\text{eff}} \nabla^2 T = 0 \tag{5}$$

where C_w is the heat capacity of the fluid, λ_{eff} is the effective thermal conductivity, and the average volumetric heat capacity of the medium is defined by $(\rho C)_{\text{avg}} = (1-n)\rho_S C_S + n\rho_w C_w$, with C_S denoting the solid heat capacity and, ρ_w and ρ_S the density of fluid and solid phases, respectively. The effective thermal conductivity is defined as $\lambda_{\text{eff}} = (1-n)\lambda_S + n\lambda_W$, in which λ_S and λ_W are the thermal conductivity coefficients of the solid and fluid phases, respectively.

In the *Local Thermal Non-Equilibrium* (LTNE) formulation, each phase has a distinct temperature at material points since the thermal equilibrium is not a priori in the LTNE. Hence, two temperature fields must be considered that can be related to each other by a heat exchange term between the two phases, coupling their energy balance equations. The heat transfer equations of the fluid and solid phases can be therefore written respectively as

$$n\rho_w C_w \frac{\partial T_w}{\partial t} + \left(\rho_w C_w \mathbf{u}_m \right) \nabla T_w - n\lambda_w \nabla^2 T_w = h_{\text{int}} \left(T_s - T_w \right) \tag{6}$$

$$\left(1-n\right) \rho_s C_s \frac{\partial T_s}{\partial t} - \left(1-n\right) \lambda_s \nabla^2 T_s = -h_{\text{int}} \left(T_s - T_w \right) \tag{7}$$

where T_W and T_S are the temperatures of the two phases, and h_{int} is the volumetric heat transfer coefficient between the matrix and fluid. Comparing the energy balance equations of the fluid phase for LTE and LTNE reveals that these two equations are very similar but with two major differences; firstly, the exchange term on the right-hand side of the LTNE equation is absent in the LTE, and secondly, the definition of coefficients differs between the two formulations. Moreover, the energy balance equation of the solid phase is absent in the LTE.

3 GOVERNING EQUATIONS OF THE FRACTURE DOMAIN

3.1 Continuity of the fluid phase

The governing equation of flow within the fracture and the matrix can be written in the same form. The mass conservation equations in the fracture domain can be obtained as

$$\alpha \nabla \mathbf{v}_s + \nabla \mathbf{u}_f + S_f \dot{p} - \beta_f \dot{T} = 0 \qquad \text{on} \quad \Omega_d \tag{8}$$

where the subscript f stands for the fractured medium. The fluid velocity in the fracture is defined as $\mathbf{u}_f = (k_f / \mu_w)(-\nabla p + \rho_w \mathbf{b}_{\Omega d})$, in which $\mathbf{b}_{\Omega d}$ is the body force in the fracture domain. The variation of fracture permeability is given based on the cubic law as $k_f = k_0 (b/b_0)^2$, where k_0 is the initial fracture permeability and, b_0 and b are the initial and current fracture aperture, respectively. Moreover, the storage coefficient is defined as $S_f = (\alpha - n_f)/K_S + n_f / K_W$, and the thermal expansion coefficient as $\beta_f = (\alpha - n_f)\beta_S + n_f \beta_W$.

3.2 Energy conservation equation

The heat transfer equation of the fracture can be written based on the LTE assumption as

$$(\rho C)_f \frac{\partial T}{\partial t} + \left(\rho_w C_w \mathbf{u}_f\right) \nabla T - \lambda_f \nabla^2 T = 0 \qquad \text{on} \quad \Omega_d \tag{9}$$

in which the average volumetric heat capacity is defined as $(\rho C)_f = (1 - n_f)\rho_S C_S + n_f \rho_w C_w$, and the average thermal conductivity as $\lambda_f = (1 - n_f)\lambda_s + n_f \lambda_w$. In a similar manner, the LTNE forms of the heat transfer equation for the fluid and solid phases can be obtained as

$$n_f \rho_w C_w \frac{\partial T_w}{\partial t} + \left(\rho_w C_w \mathbf{u}_f\right) \nabla T_w - n_f \lambda_w \nabla^2 T_w = h_{\text{int}} (T_S - T_W) \qquad \text{on} \quad \Omega_d \tag{10}$$

$$(1 - n_f)\rho_S C_S \frac{\partial T_S}{\partial t} - (1 - n_f)\lambda_S \nabla^2 T_S = -h_{\text{int}} (T_S - T_W) \qquad \text{on} \quad \Omega_d \tag{11}$$

4 THE WEAK FORMS OF GOVERNING EQUATIONS

In order to obtain the weak forms of the governing equations, multiply the admissible test functions for the displacement $\delta \mathbf{u}(\boldsymbol{x}, t)$, fluid pressure $\delta p(\boldsymbol{x}, t)$, solid temperature $\delta Ts(\boldsymbol{x}, t)$, and fluid temperature $\delta Tw(\boldsymbol{x}, t)$ fields into equations (1), (3), (6) and (7), respectively, integrate over the domain Ω, and apply the Divergence theorem, it leads to

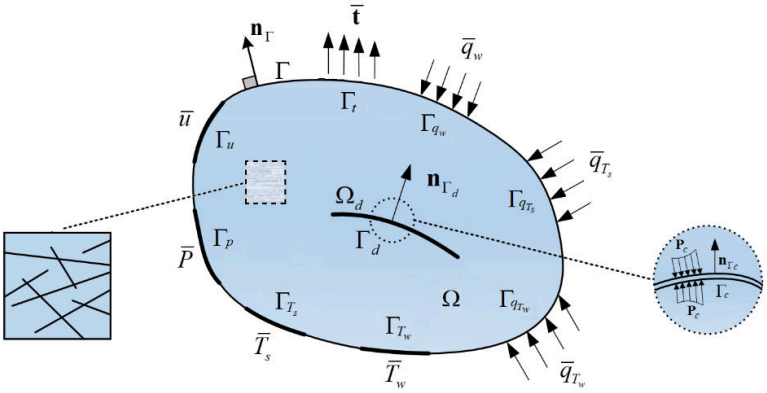

Figure 1: A fractured porous medium Ω containing large-scale fracture Γ_d and small-scale micro-fractures

$$\int_\Omega \nabla^s \delta\mathbf{u} : \boldsymbol{\sigma} d\Omega + \int_{\Gamma_c} [[\delta\mathbf{u}]]\mathbf{p}_c d\Gamma + \int_{\Gamma_d} (-\alpha p)\delta\mathbf{u}\cdot\mathbf{n}_{\Gamma d} d\Gamma + \int_\Omega \rho\delta\mathbf{u}\cdot\ddot{\mathbf{u}} d\Omega = \int_{\Gamma_t} \delta\mathbf{u}\cdot\bar{\mathbf{t}} d\Gamma + \int_\Omega \rho\delta\mathbf{u}\cdot\mathbf{b} d\Omega \tag{12}$$

$$\int_\Omega \delta p\cdot\alpha\nabla\cdot\mathbf{v}_S d\Omega + \int_\Omega \nabla\delta p\mathbf{k}_m\nabla p d\Omega + \int_\Omega \delta p\cdot S_m\dot{p} d\Omega - \int_\Omega \delta p\cdot\beta_m\dot{T} d\Omega - \int_{\Gamma_d} \delta p\cdot q_{Wd} d\Gamma = \int_\Omega \nabla\delta p\mathbf{k}_m\cdot\rho_w\mathbf{b} d\Omega - \int_{\Gamma_{q_w}} \delta p\cdot\bar{q}_W d\Gamma \tag{13}$$

$$\int_\Omega \delta T_S\left((1-n)\rho_S C_S\right)\dot{T}_S d\Omega + \int_\Omega (1-n)\lambda_S\nabla\delta T_S\cdot\nabla T_S d\Omega - \int_{\Gamma_d} \delta T_S\cdot q_{T_{Sd}} d\Gamma + \int_\Omega \delta T_S\left(h_{\text{int}}\right)T_S d\Omega - \int_\Omega \delta T_S\left(h_{\text{int}}\right)T_W d\Omega = -\int_{\Gamma_{q_s}} \delta T_S\cdot\bar{q}_{T_{Sd}} d\Gamma \tag{14}$$

$$\int_\Omega \delta T_W\left(n\rho_W C_W\right)\dot{T}_W d\Omega + \int_\Omega \delta T_W\left(\rho_W C_W\mathbf{u}_m\right)\nabla T_W d\Omega + \int_\Omega n\lambda_W\nabla\delta T_W\cdot\nabla T_W d\Omega - \int_{\Gamma_d} \delta T_W\cdot q_{T_{Wd}} d\Gamma + \int_\Omega \delta T_W\left(h_{\text{int}}\right)T_W d\Omega - \int_\Omega \delta T_W\left(h_{\text{int}}\right)T_S d\Omega = -\int_{\Gamma_{q_W}} \delta T_W\cdot\bar{q}_{T_{Wd}} d\Gamma \tag{15}$$

where $\mathbf{n}_{\Gamma d}$ denotes the unit outward normal to the fracture boundary Γ_d, and q_{Wd}, $q_{T_{Sd}}$, and $q_{T_{Wd}}$ are the fluxes transferred between the fracture domain and surrounding porous medium (**Figure 1**). The operator [[*]] represents the difference between the corresponding values at the two faces of the discontinuity. In above, the tensor $\mathbf{p}_c$ refers to the contact traction over the contact segment Γ_c of the discontinuity. In order to calculate the unknown interfacial fluxes, the coupling between the weak forms of governing equations inside and outside the fracture domain must be taken into account. In this study, an approach is employed for the coupling of micro/macro-scales of fracture equations in XFEM [14]. In this approach, it is assumed that the crack width is much smaller than its length, so the variation of continuous fields over the crack width can be neglected. It is also assumed that the discontinuous fields vary linearly from one side to the other side of the fracture [15].

It must be noted that the distribution of fracture length is not usually uniform in a reservoir, especially when there are natural fractures that are distributed as a network. In the EGS, there

are usually large-scale fractures that are brought about by industrial technics to increase the transmissivity of the reservoir. These long fractures can be connected to each other by the pre-existing natural cracks or secondary shorter fractures. In this study, the network of short cracks is modeled by the Equivalent Continuum Method to avoid excessive computational costs [3]. In the ECM, the permeability and compliance tensors of the matrix in the macro-scale are modified according to the micro-scale properties of the cracks and their distribution.

5 XFEM DISCRETIZATION

In this section, the weak forms of governing equations (12) to (15) are discretized using the local enrichment of the conventional FEM approximation space via the XFEM in the fractured elements. To this end, the nodal points, the support of which is bisected by the discontinuity, must be enriched. The displacement field is discontinuous across the fracture, which is called the strong discontinuity. The enriched approximation of the displacement field of the solid phase in the XFEM can be written using the Heaviside enrichment function as [12]

$$\mathbf{u}^h(x,t)=\sum_{I\in n^{\text{std}}}\mathbf{N}_{uI}(x)\mathbf{u}_I(t)+\sum_{J\in n^{\text{enr}}}\mathbf{N}_{uJ}(x)\frac{1}{2}\big(H_{\Gamma d}(x)-H_{\Gamma d}(x_J)\big)\tilde{\mathbf{u}}_J(t) \tag{16}$$

where $\mathbf{u}^h(x,t)$ represents the approximation function of displacement field, $\mathbf{u}_I(t)$ is the nodal displacement, $\tilde{\mathbf{u}}_J(t)$ is the enriched DOF, and $\mathbf{N}_{uI}(x)$ is the standard displacement shape functions. Furthermore, the enriched approximations of the fluid pressure and temperature can be written using the level-set distance function as

$$p^h(x,t)=\sum_{I\in n^{\text{std}}}\mathbf{N}_{pI}(x)p_I(t)+\sum_{J\in n^{\text{enr}}}\mathbf{N}_{pJ}(x)\big(D_{\Gamma d}(x)-D_{\Gamma d}(x_J)\big)R(x)\tilde{p}_J(t) \tag{17}$$

$$T_\pi^h(x,t)=\sum_{I\in n^{\text{std}}}\mathbf{N}_{T_\pi I}(x)\,T_{\pi I}(t)+\sum_{J\in n^{\text{enr}}}\mathbf{N}_{T_\pi J}(x)\big(D_{\Gamma d}(x)-D_{\Gamma d}(x_J)\big)R(x)\,\tilde{T}_{\pi J}(t)\qquad(\pi=s,w) \tag{18}$$

in which $p^h(x,t)$ and $T_\pi^h(x,t)$ are the approximation functions of pressure and temperature fields, $p_I(t)$ and $T_{\pi I}(t)$ are the standard DOFs and, $\tilde{p}_J(t)$ and $\tilde{T}_{\pi J}(t)$ are the enriched DOFs of pressure and temperature fields, respectively. In above, $\mathbf{N}_{pI}(x)$ and $\mathbf{N}_{T_\pi I}(x)$ represent the matrices of standard pressure and temperature shape functions. In relations (17) and (18), $R(x)$ is a weighting function defined to overcome the issue with the elements neighboring the enriched elements, called the blending elements, that violate the Partition of Unity conditions.

The abovementioned approximation fields can be concisely written as

$$\mathbf{u}^h(x,t)=\mathbf{N}_u^{\text{std}}(x)\,\mathbf{U}(t)+\mathbf{N}_u^{\text{enr}}(x)\,\tilde{\mathbf{U}}(t) \tag{19}$$

$$p^h(x,t)=\mathbf{N}_p^{\text{std}}(x)\,\mathbf{P}(t)+\mathbf{N}_p^{\text{enr}}(x)\,\tilde{\mathbf{P}}(t) \tag{20}$$

$$T_\pi^h(x,t)=\mathbf{N}_{T_\pi}^{\text{std}}(x)\,\mathbf{T}_\pi(t)+\mathbf{N}_{T_\pi}^{\text{enr}}(x)\,\tilde{\mathbf{T}}_\pi(t)\qquad(\pi=s,w) \tag{21}$$

where $\mathbf{N}_u^{\text{std}}(x)$, $\mathbf{N}_p^{\text{std}}(x)$ and $\mathbf{N}_{T_\pi}^{\text{std}}(x)$ are the standard shape functions and $\mathbf{N}_u^{\text{enr}}(x)$, $\mathbf{N}_p^{\text{enr}}(x)$ and $\mathbf{N}_{T_\pi}^{\text{enr}}(x)$ are the enriched shape functions of the displacement, pressure and temperature fields,

respectively. Moreover, $\mathbf{U}(t)$, $\mathbf{P}(t)$ and $\mathbf{T}_{\pi}(t)$ are the standard DOFs and $\tilde{\mathbf{U}}(t)$, $\tilde{\mathbf{P}}(t)$ and $\tilde{\mathbf{T}}_{\pi}(t)$ are the enriched DOFs of those variables. Substituting the XFEM approximation fields (19) to (21) into the weak forms of governing equations (12) to (15), the discretization of governing equations can be derived as

$$\mathbf{M}_{uu}\ddot{\mathbf{U}}+\mathbf{M}_{u\tilde{u}}\ddot{\tilde{\mathbf{U}}}+\mathbf{K}_{uu}\mathbf{U}+\mathbf{K}_{u\tilde{u}}\tilde{\mathbf{U}}-\mathbf{Q}_{uw}\mathbf{P}-\mathbf{Q}_{u\tilde{w}}\tilde{\mathbf{P}}-\mathbf{Q}_{uT_s}\mathbf{T}_s-\mathbf{Q}_{u\tilde{T}_s}\tilde{\mathbf{T}}_s=\mathbf{F}_u^{\text{ext}} \tag{22}$$

$$\mathbf{M}_{u\tilde{u}}^{\mathrm{T}}\ddot{\mathbf{U}}+\mathbf{M}_{\tilde{u}\tilde{u}}\ddot{\tilde{\mathbf{U}}}+\mathbf{K}_{u\tilde{u}}^{\mathrm{T}}\mathbf{U}+\mathbf{K}_{\tilde{u}\tilde{u}}\tilde{\mathbf{U}}-\mathbf{Q}_{\tilde{u}w}\mathbf{P}-\mathbf{Q}_{\tilde{u}\tilde{w}}\tilde{\mathbf{P}}-\mathbf{Q}_{\tilde{u}T_s}\mathbf{T}_s-\mathbf{Q}_{\tilde{u}\tilde{T}_s}\tilde{\mathbf{T}}_s+\mathbf{F}_{\tilde{u}}^{\text{int}}=\mathbf{F}_{\tilde{u}}^{\text{ext}} \tag{23}$$

$$\mathbf{M}_{wu}\ddot{\mathbf{U}}+\mathbf{M}_{w\tilde{u}}\ddot{\tilde{\mathbf{U}}}+\mathbf{Q}_{uw}^{\mathrm{T}}\dot{\mathbf{U}}+\mathbf{Q}_{\tilde{u}w}^{\mathrm{T}}\dot{\tilde{\mathbf{U}}}+\mathbf{C}_{ww}\dot{\mathbf{P}}+\mathbf{C}_{w\tilde{w}}\dot{\tilde{\mathbf{P}}}+\mathbf{C}_{wT_w}\dot{\mathbf{T}}_w+\mathbf{C}_{w\tilde{T}_w}\dot{\tilde{\mathbf{T}}}_w+\mathbf{H}_{ww}\mathbf{P}+\mathbf{H}_{w\tilde{w}}\tilde{\mathbf{P}}-\mathbf{F}_w^{\text{int}}=\mathbf{F}_w^{\text{ext}} \tag{24}$$

$$\mathbf{M}_{\tilde{w}u}\ddot{\mathbf{U}}+\mathbf{M}_{\tilde{w}\tilde{u}}\ddot{\tilde{\mathbf{U}}}+\mathbf{Q}_{u\tilde{w}}^{\mathrm{T}}\dot{\mathbf{U}}+\mathbf{Q}_{\tilde{u}\tilde{w}}^{\mathrm{T}}\dot{\tilde{\mathbf{U}}}+\mathbf{C}_{w\tilde{w}}^{\mathrm{T}}\dot{\mathbf{P}}+\mathbf{C}_{\tilde{w}\tilde{w}}\dot{\tilde{\mathbf{P}}}+\mathbf{C}_{\tilde{w}T_w}\dot{\mathbf{T}}_w+\mathbf{C}_{\tilde{w}\tilde{T}_w}\dot{\tilde{\mathbf{T}}}_w+\mathbf{H}_{w\tilde{w}}^{\mathrm{T}}\mathbf{P}+\mathbf{H}_{\tilde{w}\tilde{w}}\tilde{\mathbf{P}}-\mathbf{F}_{\tilde{w}}^{\text{int}}=\mathbf{F}_{\tilde{w}}^{\text{ext}} \tag{25}$$

$$\mathbf{C}_{T_wT_w}\dot{\mathbf{T}}_w+\mathbf{C}_{T_w\tilde{T}_w}\dot{\tilde{\mathbf{T}}}_w+\mathbf{H}_{T_wT_w}\mathbf{T}_w+\mathbf{H}_{T_w\tilde{T}_w}\tilde{\mathbf{T}}_w-\mathbf{H}_{T_wT_s}\mathbf{T}_s-\mathbf{H}_{T_w\tilde{T}_s}\tilde{\mathbf{T}}_s-\mathbf{F}_{T_w}^{\text{int}}=\mathbf{F}_{T_w}^{\text{ext}} \tag{26}$$

$$\mathbf{C}_{T_w\tilde{T}_w}^{\mathrm{T}}\dot{\mathbf{T}}_w+\mathbf{C}_{\tilde{T}_w\tilde{T}_w}\dot{\tilde{\mathbf{T}}}_w+\mathbf{H}_{\tilde{T}_wT_w}\mathbf{T}_w+\mathbf{H}_{\tilde{T}_w\tilde{T}_w}\tilde{\mathbf{T}}_w-\mathbf{H}_{\tilde{T}_wT_s}\mathbf{T}_s-\mathbf{H}_{\tilde{T}_w\tilde{T}_s}\tilde{\mathbf{T}}_s-\mathbf{F}_{\tilde{T}_w}^{\text{int}}=\mathbf{F}_{\tilde{T}_w}^{\text{ext}} \tag{27}$$

$$\mathbf{C}_{T_sT_s}\dot{\mathbf{T}}_s+\mathbf{C}_{T_s\tilde{T}_s}\dot{\tilde{\mathbf{T}}}_s+\mathbf{H}_{T_sT_s}\mathbf{T}_s+\mathbf{H}_{T_s\tilde{T}_s}\tilde{\mathbf{T}}_s-\mathbf{H}_{T_wT_s}^{\mathrm{T}}\mathbf{T}_w-\mathbf{H}_{\tilde{T}_wT_s}^{\mathrm{T}}\tilde{\mathbf{T}}_f-\mathbf{F}_{T_s}^{\text{int}}=\mathbf{F}_{T_s}^{\text{ext}} \tag{28}$$

$$\mathbf{C}_{T_s\tilde{T}_s}^{\mathrm{T}}\dot{\mathbf{T}}_s+\mathbf{C}_{\tilde{T}_s\tilde{T}_s}\dot{\tilde{\mathbf{T}}}_s+\mathbf{H}_{\tilde{T}_sT_s}\mathbf{T}_s+\mathbf{H}_{\tilde{T}_s\tilde{T}_s}\tilde{\mathbf{T}}_s-\mathbf{H}_{T_w\tilde{T}_s}^{\mathrm{T}}\mathbf{T}_w-\mathbf{H}_{\tilde{T}_w\tilde{T}_s}^{\mathrm{T}}\tilde{\mathbf{T}}_w-\mathbf{F}_{\tilde{T}_s}^{\text{int}}=\mathbf{F}_{\tilde{T}_s}^{\text{ext}} \tag{29}$$

in which the definitions of the coefficient matrices and flux vectors can be found in details in [14]. In order to complete the numerical formulation, the Generalized Newmark method can be used to discretize the system of equations in the time domain. After applying the spatial and temporal discretization into equations (22) to (29), a nonlinear system of equations can be obtained, in which the iterative Newton Raphson scheme is applied to linearize and solve the system of equations.

6 MODELING HEAT EXTRACTION FROM EGS WITH DOUBLET VERTICAL WELLS

In order to illustrate the performance of heat extraction process in EGS and the capability of the combined XFEM–ECM model for different fracture networks, a 300×300 m^2 patch of an EGS reservoir is presented between two vertical wells, as depicted schematically in **Figure 2**. The rock mass contains natural short fractures intermingling with larger fractures, which can possess non-conforming alignments. Various case studies of fracture networks are compared for the heat extraction, as shown in **Figure 3**. Each network contains six large fractures of 260 m length and 1 mm aperture. In addition, 100 short fractures are randomly distributed all over the domain with 30 m length and 0.02 mm opening. The equivalent permeability of short fractures is displayed in **Figure 4** for Networks A and B in $x-$ and $y-$ directions. The simulation is performed for the period of 40 years and the material properties of the EGS are reported in [14]. The inlet and outlet maintain average pressures of 15 and 10 MPa, respectively, and the other boundaries are set as impermeable. The initial water pressure in the reservoir is set to 10 MPa, and the reservoir temperature for both phases is initially assumed $200\,^{\circ}$C. The temperature at the injection well is $20\,^{\circ}$C, and the natural boundary conditions are set for the other boundaries. The displacement of solid phase is fixed all over the boundaries.

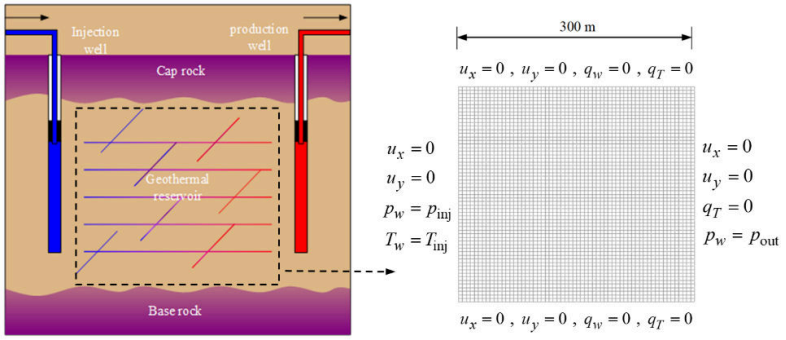

Figure 2: Schematic model of EGS with doublet vertical wells pattern

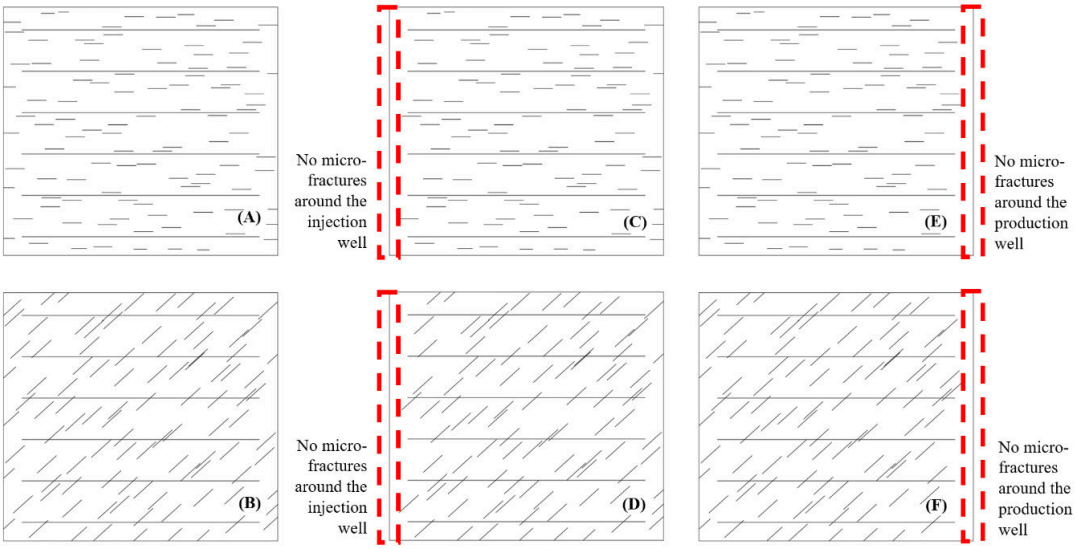

Figure 3: Different case studies of the micro-fractures alignment with macro-fractures

In **Figure 5**, the contours of temperature distribution of the reservoir are presented after 5, 20, and 40 years of injection for Networks A and B. As water flows mainly through the fractures due to higher permeability, the connected fractures form a flow network. The heat carry-over by the fluid through the fractures is obvious in this figure. Nonetheless, the fluid persists in seeping through the matrix. In addition, the fading of temperature from the fractures to the matrix can be observed; however, it should be noted that the main mechanism of heat transfer from the matrix to the fractures is conduction because the fluid velocity is low in the matrix. A comparison of the temperature distribution between the Networks A and B in **Figure 5** reveals that the better connectivity of the long and short fractures in Network B facilitates the cold water flow and accelerates the temperature drop in this network.

In order to investigate the performance of each network more quantitatively, the curves of outlet temperature and heat extraction rate are depicted in **Figure 6** at the production well during 40 years of water injection.

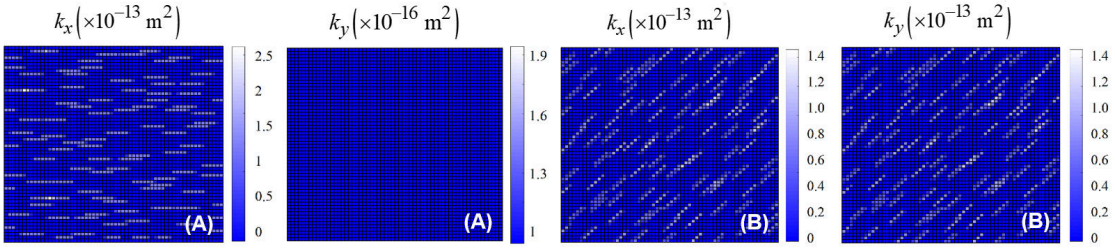

Figure 4: Distributions of equivalent permeability of micro-cracks in *x*– and *y*– directions for Networks **A** and **B**

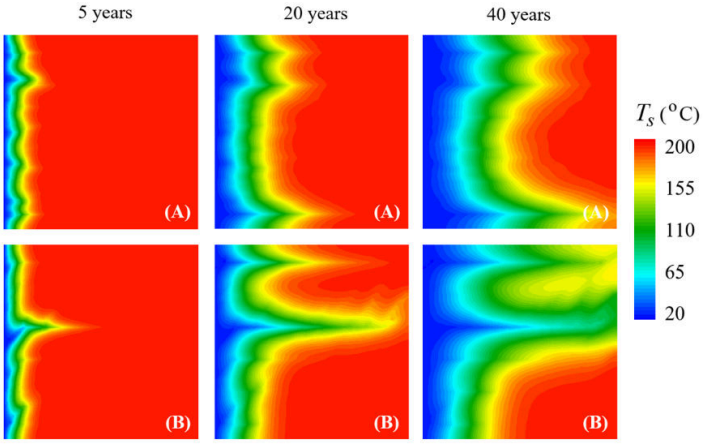

Figure 5: Contours of the temperature distribution at different times for Networks **A** and **B**

It can be seen more clearly from **Figure 6(a)** that the better connectivity of fractures in Network B outweighs the more conformity of fracture inclinations in Network A. To expand on this, it should be noted that both the connectivity and alignment of the fractures can cause an early thermal breakthrough. In Network B, the inclination of short fractures tends to divert the flow from the production well; but at the same time, it increases the connectivity by crossing the long fractures. On the other hand, all fractures are aligned with the production path in Network A, but they are not connected effectively. Furthermore, the results of the heat extraction rate are depicted in **Figure 6(b)**. The influence of fracture connectivity on the heat production can be revealed more clearly by looking at the results of Networks C to F. It can be seen from **Figure 3** that Networks C and D are respectively similar to Networks A and B, except that the first columns of connecting micro-fractures at the injection wells are removed. Similarly, the micro-fractures adjacent to the production well are removed in Networks E and F. The results of heat production rate illustrate that removing the connecting fractures at the injection well in Networks C and D can reduce the heat production rates significantly compared to Networks A and B. Finally, the effect of two different coupling conditions is investigated in **Figure 7** using the Thermo-Hydraulic (TH) and Thermo-Hydro-Mechanical (THM) models for Networks A and B. In the TH model, the solid deformation is fixed to zero and the linear momentum equation of the solid phase is ignored. Obviously, the TH model of both Networks A and B exhibits an initial shift from their base cases that can be attributed to the hydraulic effect rather than the thermal effect on the solid phase.

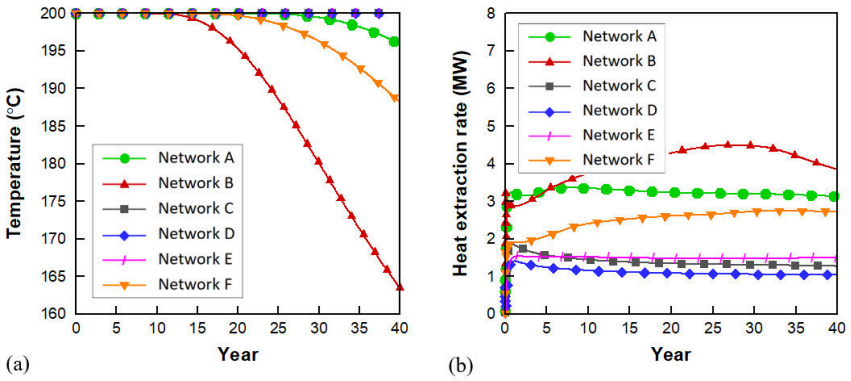

Figure 6: The time-history of (a) outlet temperature, (b) heat extraction rate at the production well for different networks of fracture density and orientation during 40 years of water injection

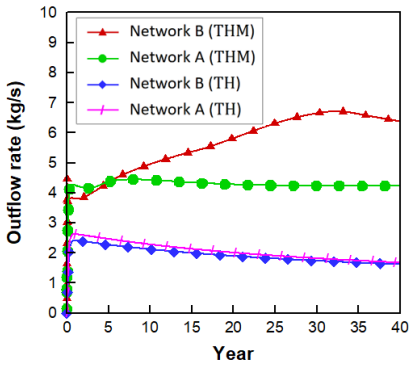

Figure 7: The time-history of outlet flow rate using different coupling conditions for Networks **A** and **B**

7 CONCLUSIONS

In this paper, a computational algorithm is presented based on a hybrid model that pursues fusing the efficiency of ECM and the accuracy of XFEM for the performance assessment of EGS. The large-scale fractures that require higher levels of accuracy and less mesh-dependence in fluid and heat exchange calculations were simulated by the XFEM, while the network of small-scale fractures was incorporated via the ECM. The set of THM equations was solved with both LTE and LTNE assumptions to find out the impact of each method on the production temperature. The simultaneous effects of fracture connectivity and inclination between two vertical wells were investigated in an EGS reservoir. Two base cases were considered where one of the networks involved a non-conforming inclination but a better connectivity of the fractures compared with the other network. Moreover, the effect of network connectivity was further investigated by removing the first layer of connecting fractures adjacent to the injection or production wells, which revealed that the influence of connectivity at the injection well is more pronounced than at the production well. It was illustrated that the network connectivity can outperform the fracture alignment and lead to an earlier thermal breakthrough. However, if the connection is poor with the main fractures, the influence of fracture alignment conformity

gets predominant. These conclusions remind that exclusive assessment of fracture networks in different EGS projects can be indispensable. It is shown that the developed model is a promising tool for the estimation of EGS performance, and it should be extended to 3D models with two-phase fluid flow to investigate the effect of other working fluids on the EGS performance.

REFERENCES

[1] Olasolo, P., Juárez, M.C., Morales, M.P., Damico, S., Liarte, I.A., Enhanced geothermal systems (EGS): A review, Renew. Sustain. *Energy Rev.* (2016) **56:** 133–144.

[2] McClure, M.W., Horne, R.N., An investigation of stimulation mechanisms in Enhanced Geothermal Systems, *Int. J. Rock Mech. Min. Sci.* (2014) **72:** 242–260.

[3] Khoei, A.R., Hosseini, N., Mohammadnejad, T., Numerical modeling of two-phase fluid flow in deformable fractured porous media using the extended finite element method and an equivalent continuum model, *Adv. Water Resour.* (2016) **94:** 510–528.

[4] Chamorro, C.R., García-Cuesta, J.L., Mondéjar, M.E., Pérez-Madrazo, A., Enhanced geothermal systems in Europe: An estimation and comparison of the technical and sustainable potentials, *Energy.* (2014) **65:** 250–263.

[5] Khoei, A.R., Mortazavi, S.M.S., Thermo-hydro-mechanical modeling of fracturing porous media with two-phase fluid flow using X-FEM technique, *Int. J. Numer. Anal. Methods Geomech.* (2020) **44:** 2430–2472.

[6] Zhang, J., Xie, J., Effect of reservoir's permeability and porosity on the performance of cellular development model for enhanced geothermal system, *Renew. Energy.* (2020) **148:** 824–838.

[7] Zhang, W., Qu, Z., Guo, T., Wang, Z., Study of the enhanced geothermal system heat mining from variably fractured hot dry rock under thermal stress, *Renew. Energy.* (2019) **143:** 855–871.

[8] Chen, Y., Ma, G., Wang, H., Heat extraction mechanism in a geothermal reservoir with rough-walled fracture networks, *Int. J. Heat Mass Transf.* (2018) **126:** 1083–1093.

[9] Khoei, A.R., Amini, D., Mortazavi, S.M.S., Modeling non-isothermal two-phase fluid flow with phase change in deformable fractured porous media using extended–FEM, *Int. J. Numer. Meth. Eng.* (2021) **122:** 4378–4426.

[10] Mortazavi, S.M.S., Pirmoradi, P., Khoei, A.R., Numerical simulation of cold and hot water injection into naturally fractured porous media using the extended–FEM and an equivalent continuum model, *Int. J. Numer. Anal. Methods Geomech.* (2022) **46:** 617–655.

[11] Hamidi, S., Heinze, T., Galvan, B., Miller, S., Critical review of the local thermal equilibrium assumption in heterogeneous porous media: Dependence on permeability and porosity contrasts, *Appl. Therm. Eng.* (2019) **147:** 962–971.

[12] Khoei, A.R., *Extended Finite Element Method: Theory and Applications,* John Wiley, 2015.

[13] Lewis, R.W., Schrefler, B.A., *The Finite Element Method in the Static and Dynamic Deformation and Consolidation of Porous Media,* John Wiley, 1999.

[14] Mortazavi, S.M.S., Beydokhti, O.R., Khoei, A.R., Modeling enhanced geothermal systems using a hybrid XFEM–ECM technique, *Appl. Therm. Eng.* (2023) **230:** 120755.

[15] Mohamadnejad, T., Khoei, A.R., Hydro-mechanical modeling of cohesive crack propagation in multiphase porous media using the extended-FEM technique, *Int. J. Numer. Anal. Methods Geomech.* (2023) **37:** 1247–1279.